Absolute Stability Analysis of a Phase Plane Controlled Spacecraft

Jiann-Woei Jang[1], Michael Plummer[2] and Nazareth Bedrossian[3]
The Charles Stark Draper Laboratory, Inc., Houston, TX, 77058

Charles Hall[4], Mark Jackson[5]
NASA Marshall Space Flight Center, Huntsville, AL, 35812

and

Pol Spanos[6]
Department of Mechanical Engineering & Material Science, Rice University, TX 77251

Many aerospace attitude control systems utilize phase plane control schemes that include nonlinear elements such as dead zone and ideal relay. To evaluate phase plane control robustness, stability margin prediction methods must be developed. Absolute stability is extended to predict stability margins and to define an abort condition. A constrained optimization approach is also used to design flex filters for roll control. The design goal is to optimize vehicle tracking performance while maintaining adequate stability margins. Absolute stability is shown to provide satisfactory stability constraints for the optimization.

Nomenclature

α	=	Lower Sector Bound
B_{RCS}	=	Thrust Direction Mapping Matrix
β_{min}	=	Required Upper Sector Limit
δ	=	Dead Zone Width
η	=	Flex Displacement
f_{Rk}	=	Force Vector from Roll Thrust k
$G(s)$	=	Open Loop Transfer Function
$G_{tr}(s)$	=	Siljak Transformed Open Loop Transfer Function
G_{xR}	=	Roll Torque about Centerline Due to All Thrusters
I_{xx}	=	Inertia
k_δ	=	Siljak Transformation Gain
k_D	=	Derivative Gain
k_P	=	Proportional Gain
μ_{RKi}	=	Displacement Vector of the i^{th} Mode at Thrust k
σ_{max}	=	Limit to Finite Domain of Absolute Stability
Ω	=	Diagonal Matrix of Flex Frequencies
ω_c	=	Crossover Frequency
ω_{RL}	=	Rate Limit
ω_{INU}	=	Sensed Rate at the INU
Φ_β	=	Mode Shapes at Jet Locations
Φ_γ	=	Mode Shapes in Roll at Output Node
ϕ	=	Roll Attitude

[1]Senior Member Technical Staff, Draper Laboratory, Houston, TX 77058; jang@draper.com, AIAA Senior Member
[2]Draper Fellow, Draper Laboratory, Houston, TX 77058, mkp2421@draper.com
[3]Group Leader, Manned Space Systems; Draper Laboratory, Houston TX, 77058: naz@draper.com
[4]Senior Aerospace Engineer; NASA Marshall Space Flight Center, Huntsville, AL 35812:Charles.E.Hall@nasa.gov
[5]Senior Aerospace Engineer; NASA Marshall Space Flight Center, Huntsville, AL 35812: mark.e.jackson@nasa.gov
[6]L. B. Ryon Professor of Mechanical and Civil Engineering, Rice University, TX 77251: spanos@rice.edu

ψ	=	Nonlinear Element Output
ψ_{tr}	=	Siljak Transformed Nonlinear Element Output
PD	=	Proportional-Derivative Control
$\rho_{\dot{\Phi}i}$	=	Rotation of the ith Mode at the Rate Gyro
σ	=	Nonlinear Element Input
T_{jets}	=	Jet Select Mapping Matrix
u_R	=	Roll Command (0,1,-1)
Z	=	Diagonal Matrix of Modal Damping Ratios

I. Introduction

The nonlinear phase plane controller, "an idealized method of treating performance optimization for classes of minimum time and/or minimum fuel problems," has been used in aerospace systems such as the Space Shuttle and the ISS for years[1, 2, 3]. Few techniques are currently available to evaluate stability margins for nonlinear control systems such as the phase plane controller. Absolute stability was utilized in a concept for stabilizing the Saturn V pitch control system[4]. Similar to describing functions, absolute stability has not been applied to a phase plane controlled system for the purpose of determining stability margins. The objective of this paper is to apply absolute stability for evaluating nonlinear controller stability and performance in phase plane controlled spacecraft. Absolute stability techniques including the circle criterion and the Popov criterion are examined and stability margin are developed. A constrained minimization approach is applied to design optimized flex filters. The design goal is to maximize bandwidth in order to optimize system performance while ensuring robust system stability margins.

II. Spacecraft Attitude Dynamics and Control

It is advantageous to limit the number of simplifications and assumptions; on the other hand, in order to concisely compare these analytical techniques, it is necessary to implement several simplifications and assumptions that limit the scope of this thesis. Frozen time analysis has proven to be effective in spacecraft with slowly varying parameters such as the Saturn V[5]. Because of this fact, only frozen time models will be considered in this paper. Aerospace attitude control systems often consist of both gimbal control and fixed jet control where the former is used for pitch and yaw control while the latter is utilized for roll control. Pitch and yaw axes have both been thoroughly explored in previous work, so this thesis will only examine the roll axis[6]. This paper operates under the assumption that there will be no aerodynamic forces exerted on the system structure in the roll axis; thereby, simplifying the rigid and flex dynamics without losing much fidelity for most aerospace systems. The dynamics equations can be split into two subsets: rigid and flex. The equation for rigid dynamics can be seen in Equation 1[7]:

$$I_{xx}\ddot{\Phi} = G_{xR} \tag{1}$$

In Equation 1, G_{xR} is the torque about the centerline due to all thrusters while I_{xx} is the inertia. In order to use this equation for analysis, it is desirable to convert the equation into state-space form as in Equation 2:

$$\begin{bmatrix}\dot{\Phi}\\ \ddot{\Phi}\end{bmatrix} = \begin{bmatrix}0 & 1\\ 0 & 0\end{bmatrix}\begin{bmatrix}\Phi\\ \dot{\Phi}\end{bmatrix} + \begin{bmatrix}0\\ G_{xR}/I_{xx}\end{bmatrix}u \tag{2}$$

Because only rate is desired in the output, the output equation is defined as such:

$$y_1 = \begin{bmatrix}0 & 1\end{bmatrix}\begin{bmatrix}\Phi\\ \dot{\Phi}\end{bmatrix} \tag{3}$$

The flex dynamics equation for the can be derived from the following dynamics equations[7]:

$$(s^2 + 2\xi_{\beta i}\omega_{\beta i}s + \omega_{\beta i}^2)\eta_{\beta i} = u_R \sum_{k}^{thrusters} f_{Rk}^T \mu_{Rki} \tag{4}$$

In Equation 4, $\xi_{\beta i}$ is the damping ratio of the i^{th} mode, $\omega_{\beta i}$ is the flex frequency of the i^{th} mode, $\eta_{\beta i}$ is the flex diplacement of the i^{th} mode, u_R is the roll command (0,1,-1), f_{Rk}^T is the force vector from roll thrust k, and μ_{Rki} is the displacement vector of the i^{th} mode at thrust k[7]. The state-space representation for the flex system can be seen in Equations 5 and 6[7]:

$$\begin{bmatrix} \dot{\eta} \\ \ddot{\eta} \end{bmatrix} = \begin{bmatrix} 0 & 1 \\ -\Omega_\beta^2 & -2Z_\beta\Omega_\beta \end{bmatrix} \begin{bmatrix} \eta \\ \dot{\eta} \end{bmatrix} + \begin{bmatrix} 0 \\ \Phi_\beta B_{RCS} T_{jets} \end{bmatrix} u \tag{5}$$

$$y_2 = \begin{bmatrix} 0 & \Phi_\gamma \end{bmatrix} \begin{bmatrix} \eta \\ \dot{\eta} \end{bmatrix} \tag{6}$$

In Equation 5 and 6, Ω_β is a diagonal matrix of flex frequencies, Z_β is a diagonal matrix of damping ratios, Φ_β^T is the mode shapes at jet locations, B_{RCS} is the thrust direction mapping matrix, T_{jets} is the jet select mapping matrix, and Φ_γ is the mode shape at the output node. The final governing equation that will be discussed in this section is the sensor output equation which reflects how the flex dynamics affect the readings to which the controller responds[7].

$$\omega_{RGA} = \phi + \sum_{i=1}^{N} \rho_{\phi i} \eta_i s \tag{7}$$

In Equation 7, ω_{RGA} is the sensed rate at the inertial navigation unit and $\rho_{\phi i}$ is the rotation of the i^{th} mode at the rate gyro. Because the high-frequency flex dynamics possess the ability to make the system unstable, it is critical that a low pass filter be employed to attenuate high-frequency flex modes. The rigid and bending plant dynamics are integrated with the flex filter and phase plane controller to create the roll dynamics and control system. The block diagram in Figure 1 outlines the dynamics and control components:

Figure 1: Dynamics and Control Block Diagram

The flex filter block includes a low-pass filter to attenuate high-frequency noise while at the same time allowing low-frequency dynamics to feedback into the controller. A phase plane control system regulates attitude tracking and performance. The phase plane controller is an inherently nonlinear system which necessitates the requirement for nonlinear techniques in order to predict the system's behavior. The phase plane controller is "an idealized method of treating performance optimization for classes of minimum time and/or minimum fuel problems"[1]. The phase plane controller offers a unique method for attitude control while responding to the vehicle dynamics in the plane defined by state errors and state rate errors. The trajectories in the phase plane can be described through Equations 8 and 9[8].

$$\phi_2 = \phi_2 + \omega\Delta t \tag{8}$$

$$\dot{\phi}_2 = \dot{\phi}_2 + \alpha\Delta t \tag{9}$$

In the expressions above ω is angular velocity, α is angular acceleration, and Δt is the thruster firing time for the phase plane controller. Figure 2 demonstrates how trajectories in the phase plane operate. For example, consider the starting point in Figure 2. The system applies a continuous torque until it enters the drift channel. At this point, the thrusters discontinue their firing and the system's attitude continues to increase because the system is

in the upper half of the phase plane which means it has a positive rate. The rate is constant as long as there is no firing because the system cannot accelerate. Once the system crosses the negative switch line into the negative firing region, the system undergoes a negative acceleration which places the system back into the non-firing region; however, the system's attitude will continue to move towards the negative firing region until the system has been driven into the lower half of the phase plane. Once there, the system's attitude will decrease in the non-firing region until it crosses the positive switch line at which point a positive firing will occur[8].

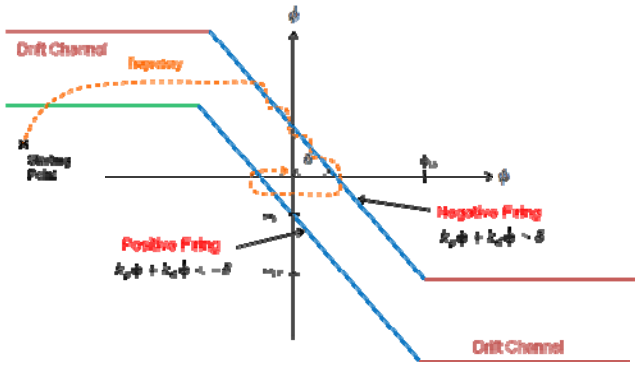

Figure 2: The Phase Plane Controller

The system will continue to oscillate around the origin of the phase plane in what is called a limit cycle. A common definition of a limit cycle is an oscillation of "fixed amplitude and fixed period without external excitation"[9]. In order to evaluate a nonlinear system such as a phase plane controlled system, it is necessary to transform the phase plane controller into a form where control techniques can be applied. This will be accomplished in a two step process. First, only the attitude hold region will be evaluated, and second, the phase plane controller will be transformed into an equivalent system consisting of a PD controller and a nonlinear element consisting of a dead zone and an ideal relay. This development can be seen in Figure 3:

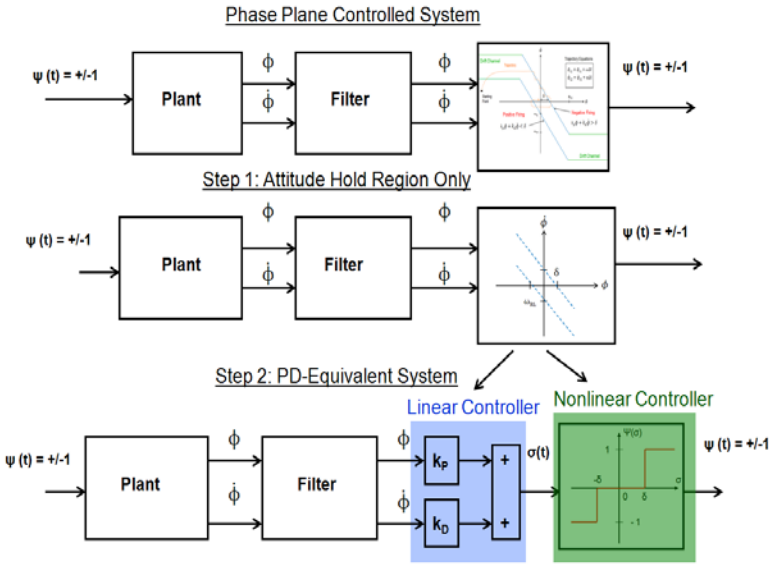

Figure 3: PD-Equivalent Phase Plane Development

In Figure 3, step one ignores the drift channels of the phase plane controller because this thesis will focus on the sloped portion of the phase plane. The two switching curves, which define the dead zone between the positive and negative firing regions, can be defined by the inequality:

$$-(\omega_{RL}/\delta)\phi - \omega_{RL} < \dot{\phi} < -(\omega_{RL}/\delta)\phi + \omega_{RL} \tag{10}$$

In order to progress from step two to step three in Figure 3, it is necessary to implement a PD controller. It is first necessary to rewrite Equation 10:

$$-1 < \phi/\delta + \dot{\phi}/\omega_{RL} < 1 \tag{11}$$

Multiplying Equation 11 by the dead zone, δ, leads to Equation 12:

$$-\delta < \phi + (\delta/\omega_{RL})\dot{\phi} < \delta \tag{12}$$

This inequality provides the following values for k_P and k_D which are the proportional and derivative gains respectively[8].

$$k_P = 1 \tag{13}$$

$$k_D = \delta/\omega_{RL} \tag{14}$$

The k_p and k_d values calculated above are instrumental in creating a practical phase plane controller that can be used with control analysis techniques. Substituting these values into Equation 12 yields the result for the dead zone[8].

$$-\delta < k_P\phi + k_D\dot{\phi} < \delta \tag{15}$$

The phase plane controller utilizes thruster firings. To model these firings, it is necessary to switch the signs from Equation 15 which models the dead zone. The thrusters are activated whenever either of the two inequalities becomes true[8].

$$k_P\phi + k_D\dot{\phi} < -\delta \text{ [Positive Firing]} \tag{16}$$

$$k_P\phi + k_D\dot{\phi} > \delta \text{ [Negative Firing]} \tag{17}$$

The nonlinear controller portion in step three of Figure 3 can be evaluated by nonlinear control analysis techniques such as absolute stability.

III. Absolute Stability

The phase plane controller is a nonlinear control scheme which means it is necessary to take these nonlinearities into account when determining system stability. Absolute stability provides a method for guaranteeing asymptotic stability for a nonlinear system primarily through two techniques called the circle criterion and the Popov criterion. Both the circle criterion and the Popov criterion were developed in the 1960's by theorists such as Zames and Popov who applied Lyapunov's second method to the frequency domain[10, 11]. For systems with nonlinearities such as dead zone and ideal relay, standard linear control methodologies such as Bode and Nichols cannot be applied. These nonlinear aspects must be taken into account. The Lur'e Problem accomplishes this task by separating the linear and nonlinear elements as in the Figure 5[12]:

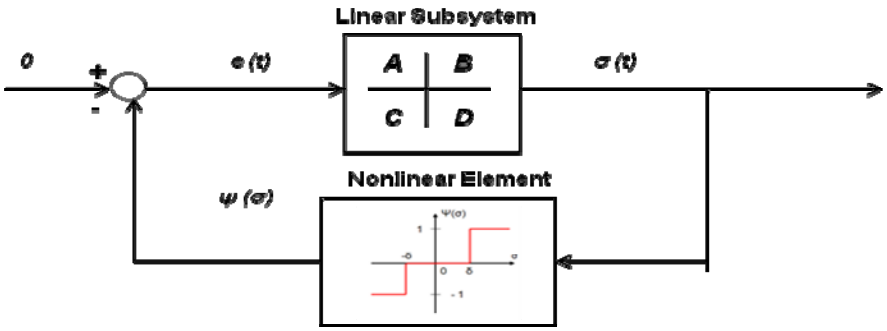

Figure 5: Lur'e Problem System Model

Figure 5 corresponds to the following system of equations[12]:

$$\dot{x} = Ax + B\psi(\sigma) \tag{18}$$

$$\sigma = Cx \tag{19}$$

Using this model, it is possible to evaluate the sector bounds for the nonlinear element. A nonlinearity belongs to a sector [α, β], where β and α are the upper and lower sector bounds respectively, if the inequality holds true[12]:

$$\alpha\sigma^2 < \psi(\sigma)\sigma < \beta\sigma^2 \tag{20}$$

Sector bounds define the regions where a nonlinearity can dwell when plotting the input, $\sigma(t)$, versus the output, $\psi(\sigma)$ as in Figure 6[12]:

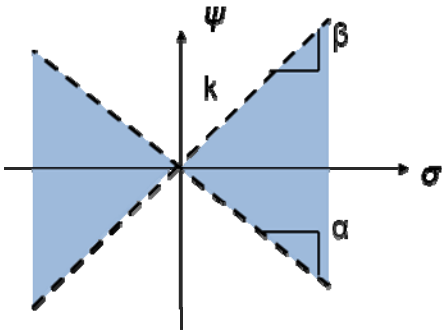

Figure 6: Input/Output Sector Bounds

These sector bounds allow for nonlinear stability to be ascertained by way of frequency-based methods such as the circle criterion and Popov criterion. A system with nonlinearities enclosed within the sector bound is guaranteed to be asymptotically stable provided the system is a minimal realization of *G(s)*. This means that the **A** and **C** matrices must be observable while the **A** and **B** matrices must be controllable when the system is in state space form[12]. Determining β and α can be accomplished through one of three cases, collectively known as the Circle Criterion. In this paper only the second case will be considered. The linear system, *G(s)*, must be strictly Hurwitz which means all poles are in the open left hand side of the s-plane. The Nyquist plot of *G(s)* must lie to the "right of the vertical line defined by Re[s] = -1/β"[13]. The Popov criterion is an additional method for determining whether or not a nonlinear system possesses absolute stability. As in the circle criterion, it is necessary to begin with the Lur'e problem system setup in Figure 5. There are limitations to the particular type of system that can use the Popov criterion to ensure absolute stability. Vidyasagar notes "unlike the circle criterion, the Popov criterion is applicable only to *autonomous* systems"[12]. An autonomous system is defined as autonomous if *f* in the following expression "does not depend explicitly on time"[14]. That is:

$$\dot{x} = f(x) \tag{21}$$

A system that is non-autonomous would have behavior that could be described by Equation 22[14]:

$$\dot{x} = f(x,t) \tag{22}$$

As in the circle criterion, it is necessary that the **A** and **B** matrices are controllable and the **A** and **C** matrices are observable, therefore, ensuring the open loop transfer function for the system is a minimal realization of the system[12]. Similar to conditions two and three of the circle criterion, it is necessary for the system to be strictly Hurwitz to satisfy the Popov criterion[14]. Popov's criterion is similar to condition two of the circle criterion in that the lower sector bound, α, is set equal to zero while the upper sector bound, β, is determined through a graphical-frequency based technique. From here it is necessary to examine the following inequality. The inequality must be satisfied in order for absolute stability to exist[12]:

$$\mathrm{Re}[(1+j\omega r)G(j\omega)] + \frac{1}{\beta} \geq \varepsilon \quad \forall \omega \geq 0 \tag{23}$$

In Equation 23, the value ϵ should be an arbitrarily small value while r is required to be non-negative[12]. Applying constrained minimization to minimize $1/\beta$ in the above expression results in a solution for β for a

particular transfer function. The Popov plot only considers positive frequencies (unlike circle criterion plots) and is similar to the s-plane except that the Popov plot graphs Re[$G(j\omega)$] vs. ωIm[$G(j\omega)$] as opposed to Re[$G(j\omega)$] vs. Im[$G(j\omega)$] as in the circle criterion[12]. It is important to note that sector bounds generated for a given transfer function using the Popov criterion will be less conservative than those generated utilizing the circle criterion. Another significant difference between the two absolute stability criterions is that the circle criterion proves global exponential stability while the Popov criterion only guarantees global asymptotic stability[14]. To effectively compare nonlinear stability techniques, it is necessary to develop a method for determining stability margins. With absolute stability it is possible to predict gain margins through the following process. This method will be valid for absolute stability techniques such as circle criterion (case 2) or the Popov criterion. It is necessary to determine from the nonlinear element the required upper sector limit, β_{min}, as is demonstrated in Figure 9:

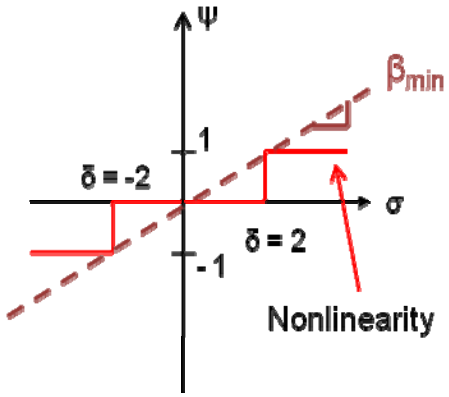

Figure 9: Determining the Required Upper Sector Limit, κ

The difference between β and β_{min} results in a gain margin region, in which the system is absolutely stable. As long as $\beta \geq \beta_{min}$, the system is considered to be stable. This region is depicted for circle criterion in Figure 10:

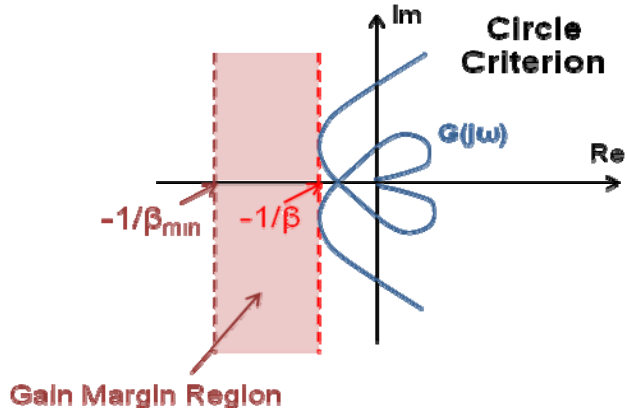

Figure 10: Gain Margin Region for Circle Criterion

The same region is illustrated for the Popov criterion in Figure 11:

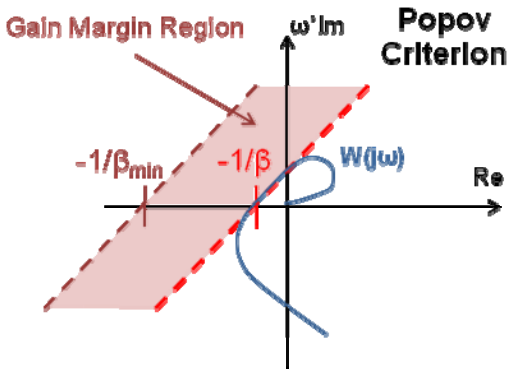

Figure 11: Gain Margin Region for Popov Criterion

Taking advantage of this gain margin region, Equation 24 is developed to determine the gain margin for a particular system.

$$\text{Gain Margin} = dB(\beta / \beta_{\min}) \tag{24}$$

IV. Finite Domain of Absolute Stability

As stated earlier, the circle criterion (case 2) and the Popov criterion require the state-space A matrix to be strictly Hurwitz. Siljak's transformation method circumvents this requirement by introducing a feedback gain which creates a transformed Hurwitz system[4]. Starting with the Lur'e system shown in Figure 4.1, the linear time-invariant (LTI) system's minimal realization transfer function leads to the following loop transformation model when Siljak's method is applied[4]:

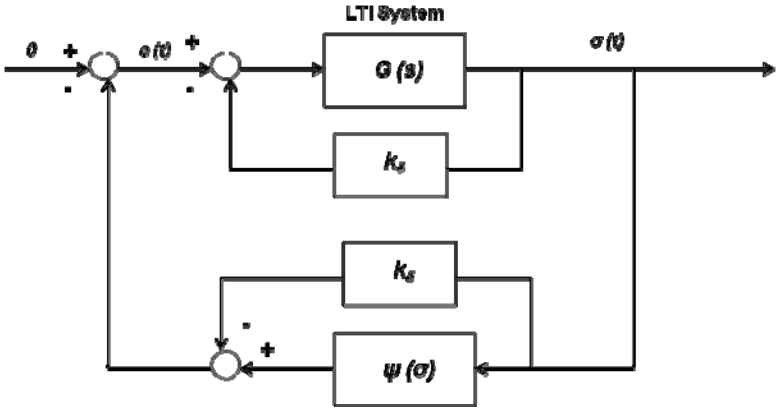

Figure 9: Loop Transformation

The above loop transformation results in the following expression for the transformed system[4]:

$$G_{tr}(s) = \frac{G(s)}{1 + k_{\delta} G(s)} \tag{25}$$

Using Equation 25, k_{δ} should be varied until $G_{tr}(s)$ is strictly Hurwitz. The transformed **A** matrix can be seen in Equation 26[4]:

$$A_{tr} = A + k_{\delta} BC \tag{26}$$

The transformed nonlinearity can be seen in the expression[4]:

$$\psi_{tr}(\sigma) = \psi(\sigma) - k_{\delta}\sigma \tag{27}$$

Because of the feed-forward element to the nonlinear output, there will be a limit on $\sigma(t)$, denoted as σ_{max}, where any input greater than that limit will lead to a sector violation. This means a system with an input greater than σ_{max} will not be guaranteed absolute stability. The new transformed state space system is seen in the form[4]:

$$\dot{x} = A_{tr}x + B\psi_{tr}(\sigma) \tag{28}$$

$$\sigma = Cx \tag{29}$$

The sector limits ($\alpha = 0$, β) are still determined by applying case two of the circle criterion or the Popov criterion to the non-transformed system. These sectors can be shown in the following inequality[4]:

$$0 \le \sigma\psi_{tr}(\sigma) \le \beta\sigma^2 \qquad \text{where } |\sigma| < \sigma_{\max} \text{ and } \psi_{tr}(0) = 0 \tag{30}$$

The Siljak transformation's main benefit is it allows the control designer to establish absolute stability over a finite domain. Whether or not a region possesses asymptotic stability depends on the type of nonlinearity which needs to be accounted for through absolute stability. Because of the negative portion in the nonlinear function equation, dead zone regions do not possess guaranteed absolute stability over a finite domain even using the Siljak transformation. This is because the sector bounds would be immediately violated as soon a $\sigma(t)$ was greater than zero, but ideal relay nonlinearities do not suffer from the same handicap. Ideal relays result in asymptotic stability because the nonlinearity has a positive slope at the origin; therefore, $\sigma_{max} > 0$ for ideal relay nonlinearities and a finite domain of absolute stability exists. Figure 10 demonstrates the concept that dead zone regions do not posses absolute stability while ideal relay regions possess absolute stability over a finite domain. In the figure below the transformed system is not guaranteed to be absolutely stable when the transformed nonlinearity enters the second or fourth quadrant.

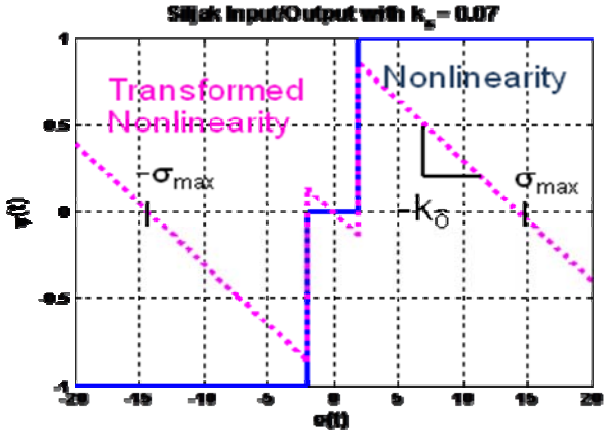

Figure 10: Siljak Transformed Input/Output

The results of the Siljak transformation with respect to dead zone and ideal relay match how the phase plane controller is designed to operate. When the system is in the dead zone region there is no firing only drifting compared to when the system is in the ideal relay portion it is firing and asymptotically stable.

V. Constrained Flex Filter Optimization

The purpose of flex filter optimization is to maximize the performance of the system while ensuring that all constraints imposed by stability and flex margin requirements are still met. An approach similar to that followed by Jang, Hall and Bedrossian will be taken in this paper[15]. A numerical optimization code is developed utilizing MATLAB's 'fmincon' function to perform a constrained minimization. Before optimization is performed, it is necessary to design initial conditions to implement as an initial filter. Ideally, any values could be selected and the optimization code would still work, but experience has shown that providing a good initial estimate improves the optimization's performance. The optimization is performed with the goal being to maximize the bandwidth of the system. This is accomplished by minimizing to following expression.

$$f = -bandwidth(G) \tag{31}$$

This minimization is constrained by the need for the system to be Hurwitz, the frequencies and damping ratios must be positive, the flex filter must achieve 30 dB of attenuation at frequencies within the stopband, and the open loop system must have 6 dB of rigid gain margin. For the filter designed using absolute stability, gain margin can be guaranteed through the constraint.

$$\min \mathrm{Re}(G_{tr}(s)) = \min \mathrm{Re}\left(\frac{G(s)}{1+k_{\delta}G(s)}\right) \geq 1 \tag{32}$$

The circle criterion is used for this calculation instead of the Popov criterion for several reasons. The first reason is that the circle criterion requires less computational resources than the Popov criterion due to the Popov criterion's use of 'fmincon'. An additional motive for using the circle criterion is that using a 'fmincon' function within another 'fmincon' function appears to create inaccuracies in the numerical optimization code and output. The requirements and design criteria are condensed in Figure 11:

minimize	-bandwidth[*F(s)*]		
subject to			
	$\min \mathrm{Re}(G_{tr}(s)) \geq 1$	$\forall \omega$	Absolute Stability
	$\lvert F(s)) \rvert < 0\,dB$	$\forall \omega < \omega_c$	Rigid Gain Stability
	$\lvert F(s)) \rvert < -30\,dB$	$\forall \omega < \omega_c$	Flex Gain Stability
	$\omega_i > 0$	i = 1, 2, 3, …	Filter Stability
	$\zeta_i > 0$	i = 1, 2, 3, …	
where			
	F(s) = Flex Filter		
	G(s) = Linear System Transfer Function		
	$G_{tr}(s) = \frac{G(s)}{1+k_{\delta}G(s)}$		
	k_{δ} = Siljak Gain		
	ω_c = Crossover Frequency (rad/sec)		

Figure 11: Optimization Criteria

A 6th order flex filter was obtained through constrained minimization and the resulting figure can be seen below in Figure 12:

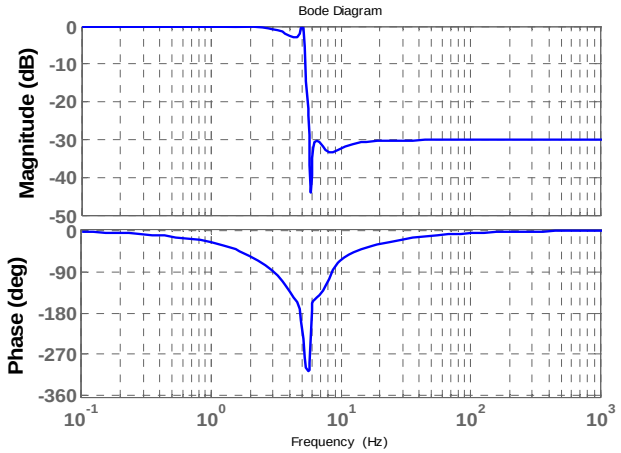

Figure 12: Absolute Stability Optimized Flex Filter

The absolute stability filter has a bandwidth of 5.17 Hz; furthermore, Figure 12 demonstrates that the filter successfully achieves 30 dB of stopband attenuation. Because the Siljak transformation is used in the absolute stability analysis, it is necessary to determine the finite domain of absolute stability. The first step is to perform a linear analysis to find the minimum k_δ value necessary to transform the phase plane control system into a Hurwitz system.

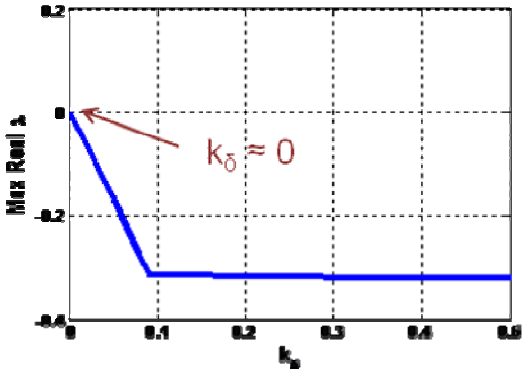

Figure 13: Linear k_δ Analysis

For this particular case, the k_δ required is so small that is can be considered to be zero. Now that k_δ has been determined, it is now necessary to plot the transformed nonlinearity to find the σ_{max} which defines the maximum input amplitude the nonlinear element can sustain before it becomes unstable.

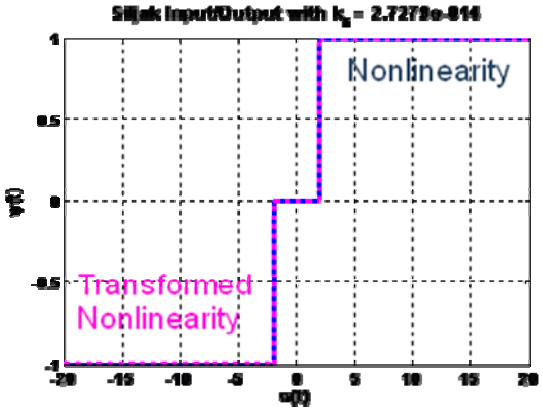

Figure 14: Input/Output Plot for Finite Domain Determination

From Figure 14 it can be noted that $\sigma_{max} = \infty$ which means that there will be no practical finite domain of absolute stability for the nominal case. Using time domain simulation, it should be noted the system maintains stability an extremely large input, $\sigma = 287.2$, in the nominal case.

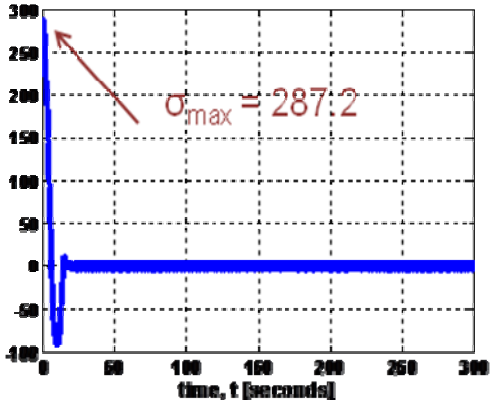

Figure 15: Time Domain Test for Finite Domain of Absolute Stability

This result indicates $\sigma_{max} \approx \infty$ for the spacecraft dynamics examined in this paper; therefore, the finite domain of absolute stability does not need to be utilized as an abort condition for the system in this case. Now that it has been confirmed no abort condition is necessary for the system, absolute stability for the new system with the optimized filter must be verified. Figure 16 displays the Popov plot showing the results for the optimized filter.

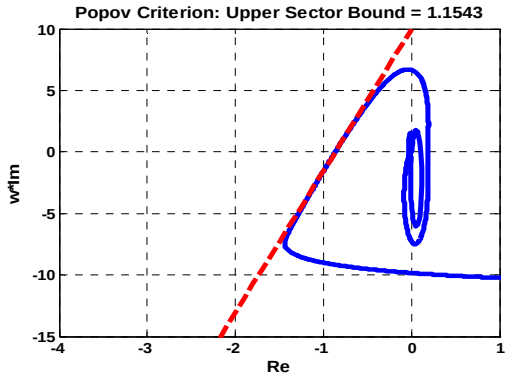

Figure 16: Popov Criterion

The Popov plot in Figure 16 shows the worst case scenario for Popov stability, and it can be seen using Equation 24 the worst case upper sector limit, $\beta = 1.15$ which corresponds to 7.6 dB of gain margin.

VI. Closure

The phase plane controller offers an idealized method for optimizing time and fuel performance while ensuring stability and attitude tracking. The circle criterion and the Popov criterion offer methods for determining not only the stability of a system but also how much gain robustness the system contains. The Popov criterion combined with Siljak's loop transformation accounts for both the dead zone and ideal relay nonlinearities. Tests indicated $\sigma_{max} \approx \infty$ for spacecraft dynamics examined in the paper; therefore, the finite domain of absolute stability does not need to be utilized as an abort condition in this system. The nonlinear analysis techniques discussed above can also be used to design optimized filters with improved performance over the current filter. A 6^{th} order filter was designed to maximize bandwidth while ensuring adequate stability. The primary constraints for the filter design were 30 dB attenuation in the stopband, 0 dB gain in the passband, 6 dB gain margin for the rigid dynamics, and 10 dB attenuation of high-frequency flex dynamics. The technique created a filter that utilized nonlinear control gain margins while ensuring maximized performance.

References

[1]Penchuk, A., P. Hattis, and E. Kubiak, "A Frequency Domain Stability Analysis of a Phase Plane Control System," Journal of Guidance, Vol. 8, No. 1, 1984.

[2]Hall, R., Barrington, R., K. Kirchwey, A. Alaniz, and K. Grigoriadis, "Shuttle Stability and Control During the Orbiter Repair Maneuver," AIAA Guidance, Navigation, and Control Conference and Exhibit, San Francisco, CA, August 2005, AIAA 2005-5852.

[3]Bedrossian, N., J. Jang, A. Alaniz, M. Johnson, K. Sebelius, and Y. Mesfin, "International Space Station US GN&C Attitude Hold Controller Design for Orbiter Repair Maneuver," AIAA GNC Conference, Monterrey, CA, 2005.

[4]Siljak D. and S. M. Setzer, "Absolute Stability Analysis of Attitude Control Systems for Large Boosters," Journal of Spacecraft and Rockets, Vol. 9, No. 7, July 1972.

[5]Greensite, A., Analysis and Design of Space Vehicle Flight Control Systems, United States: Spartan Books, 1970.

[6]Jang, J., Van Tassell, C., and Bedrossian, N., "Evaluation of Ares-I Control System Robustness to Uncertain Aerodynamics and Flex Dynamics," AIAA GN&C Conference, Honolulu, HI, 2008, AIAA-2008-6621.

[7]Frosch, James A., and Donald P. Vallely, "Saturn AS-501/S-IC Flight Control System Design," Journal of Spacecraft, Vol. 4, No. 8, August 1967.

[8]Wertz, J., *Spacecraft Attitude Determination and Control*, Boston, MS: D. Reidel Publishing Company, 1995.

[9]Gelb, A., and W. Vander Velde, *Multiple-Input Describing Functions and Nonlinear System Design*, New York, NY: McGraw-Hill Book Co., 1968.

[10]Zames, G., "On the Input-Output Stability of Time-Varying Nonlinear Feedback Systems Part I and II," IEEE Transactions on Automatic Control, Vol. AC-11, No. 2-3, April-July 1966.

[11]Popov, V.M., "Absolute Stability of Nonlinear Systems of Automatic Control," Automation and Remote Control, 22, 1961.

[12]Vidyasagar, M., *Nonlinear Systems Analysis, 2nd Edition*, Englewood Cliffs, NJ: Prentice-Hall, Inc., 2002.

[13]Khalil, H., *Nonlinear Systems, 3rd Edition*, Upper Saddle River, NJ: Prentice-Hall, Inc., 2001.

[14]Slotine, J. and W. Li, *Applied Nonlinear Control*, Upper Saddles Rive, NJ: Prentice-Hall, Inc., 1969.

[15]Jang, J., Hall, R., Bedrossian, N., and Hall, C., "Ares-I Bending Filter Design Using A Constrained Optimization Approach," AIAA GN&C Conference, August 2008.